NeuroImage: Clinical 31 (2021) 102711

Contents lists available at ScienceDirect

NeuroImage: Clinical

journal homepage: www.elsevier.com/locate/ynicl

Resting-state electroencephalographic biomarkers of Alzheimer's disease

Giordano Cecchetti [a,b,c,d,e,1], Federica Agosta [a,d,e,2], Silvia Basaia [d,3], Camilla Cividini [d,e,4], Marco Cursi [b,5], Roberto Santangelo [a,b], Francesca Caso [a,6], Fabio Minicucci [b], Giuseppe Magnani [a], Massimo Filippi [a,b,c,d,e,*,7]

[a] Neurology Unit, IRCCS San Raffaele Scientific Institute, Via Olgettina 60, 20132 Milan, Italy
[b] Neurophysiology Service, IRCCS San Raffaele Scientific Institute, Via Olgettina 60, 20132 Milan, Italy
[c] Neurorehabilitation Unit, IRCCS San Raffaele Scientific Institute, Via Olgettina 60, 20132 Milan, Italy
[d] Neuroimaging Research Unit, Division of Neuroscience, IRCCS San Raffaele Scientific Institute, Via Olgettina 60, 20132 Milan, Italy
[e] Vita-Salute San Raffaele University, Via Olgettina 60, 20132 Milan, Italy

ARTICLE INFO

Keywords:
Alzheimer's disease
EEG
eLORETA
MRI
Graph analysis
AD biomarkers

ABSTRACT

Objective: We evaluated the value of resting-state EEG source biomarkers to characterize mild cognitive impairment (MCI) subjects with an Alzheimer's disease (AD)-like cerebrospinal fluid (CSF) profile and to track neurodegeneration throughout the AD continuum. We further applied a resting-state functional MRI (fMRI)-driven model of source reconstruction and tested its advantage in terms of AD diagnostic accuracy.

Methods: Thirty-nine consecutive patients with AD dementia (ADD), 86 amnestic MCI, and 33 healthy subjects enter the EEG study. All ADD subjects, 37 out of 86 MCI patients and a distinct group of 53 healthy controls further entered the fMRI study. MCI subjects were divided according to the CSF phosphorylated tau/β amyloid-42 ratio (MCIpos: $\geq$ 0.13, MCIneg: $<$ 0.13). Using Exact low-resolution brain electromagnetic tomography (eLORETA), EEG lobar current densities were estimated at fixed frequencies and analyzed. To combine the two imaging techniques, networks mostly affected by AD pathology were identified using Independent Component Analysis applied to fMRI data of ADD subjects. Current density EEG analysis within ICA-based networks at selected frequency bands was performed. Afterwards, graph analysis was applied to EEG and fMRI data at ICA-based network level.

Results: ADD patients showed a widespread slowing of spectral density. At a lobar level, MCIpos subjects showed a widespread higher theta density than MCIneg and healthy subjects; a lower beta2 density than healthy subjects was also found in parietal and occipital lobes. Evaluating EEG sources within the ICA-based networks, alpha2 band distinguished MCIpos from MCIneg, ADD and healthy subjects with good accuracy. Graph analysis on EEG data showed an alteration of connectome configuration at theta frequency in ADD and MCIpos patients and a progressive disruption of connectivity at alpha2 frequency throughout the AD continuum.

Conclusions: Theta frequency is the earliest and most sensitive EEG marker of AD pathology. Furthermore, EEG/fMRI integration highlighted the role of alpha2 band as potential neurodegeneration biomarker.

Abbreviations: ADD, Alzheimer's disease dementia; DMN, Default Mode Network; ICA, Independent component analysis; LLC, Linear lagged connectivity; MCI, Mild cognitive impairment (pos = pTau/Aβ42≥0.13, neg = pTau/Aβ42<0.13); PVN, Primary Visual Network; RFP, Right Frontal-Parietal Network; RS-EEG, resting-state electroencephalogram; RS-fMRI, resting-state functional MRI; VISASS, Visual-Associative Network.

* Corresponding author at: Neurology Unit, Division of Neuroscience, IRCCS San Raffaele Scientific Institute, Via Olgettina 60, 20132 Milan, Italy.
E-mail address: filippi.massimo@hsr.it (M. Filippi).
[1] Cecchetti, Giordano: https://orcid.org/0000-0002-6544-410X
[2] Agosta, Federica: https://orcid.org/0000-0003-3121-4979
[3] Basaia, Silvia: https://orcid.org/0000-0002-0722-6243
[4] Cividini, Camilla: https://orcid.org/0000-0003-0602-5375
[5] Cursi, Marco: https://orcid.org/0000-0002-7928-0417
[6] Caso, Francesca: https://orcid.org/0000-0002-3072-1218
[7] Filippi, Massimo: https://orcid.org/0000-0002-5485-0479

https://doi.org/10.1016/j.nicl.2021.102711
Received 10 February 2021; Received in revised form 21 April 2021; Accepted 26 May 2021
Available online 29 May 2021

1. Introduction

Alzheimer's disease (AD) is the most common cause of dementia worldwide, accounting for up to 75–80% of cases (Qiu et al., 2009). Through the years, the need for an early diagnosis, combined with the non-optimum accuracy of pure clinical diagnosis (estimated sensitivity of 81% and specificity of 70%) (Knopman et al., 2001), progressively led to codifying AD on the basis of *in vivo* biomarkers of amyloidopathy (A; i.e., reduced cerebrospinal fluid [CSF] β amyloid [Aß42] and/or positive brain amyloid positron emission tomography scan [PET]), tauopathy (T; i.e, increased CSF hyperphosphorylated tau protein [pTau] and/or positive brain tau PET), and neurodegeneration (N; i.e., increased CSF total tau protein [tTau], positive brain 18F-fluorodeoxyglucose PET [FDG-PET], atrophy on brain magnetic resonance imaging [MRI]) (Jack et al., 2018). Within this new framework, a patient can be diagnosed with AD only in case of both positive A and T biomarkers (A+/T +). Most of the considered markers are nevertheless expensive, poorly available in clinical practice, and relatively invasive.

In this context, considering the high cost-effectiveness, availability and low invasiveness of the technique, EEG-based biomarkers have been extensively investigated in the diagnosis of AD (Cassani et al., 2018; Rossini et al., 2020). In the last decade, advanced cortical source mapping algorithms have been applied to estimate the location and distribution of active electric current sources within the brain based on the potential recorded through scalp electrodes (Rossini et al., 2020; Babiloni et al., 2020). Among other algorithms, exact low-resolution brain electromagnetic tomography (eLORETA) solutions (Pascual-Marqui, 2007a) have been previously used and demonstrated to significantly correlate with neuropsychological deficits and MRI hippocampal volume in AD patients (Babiloni et al., 2009, 2013). More recently, new advances in resting-state analysis techniques have shown the possibility of examining the overall structure of the brain network using graph analytical methods and time-series of eLORETA values have been implemented in connectomics studies of AD and physiological ageing (Rossini et al., 2020; Rubinov and Sporns, 2010; Vecchio et al., 2014, 2017, 2018). In particular, the functional connected brain network can be represented as a graph, consisting of nodes, and edges (or connections) between regions that are functionally linked; on this basis, it can be described by specific parameters of segregation (e.g., clustering coefficient) and integration (e.g., characteristic path length) (Rossini et al., 2020; Rubinov and Sporns, 2010; Vecchio et al., 2014, 2017, 2018).

Within this context, the aim of our study was to investigate the value of 19-channel resting state EEG (RS-EEG) source biomarkers in correctly classifying mild cognitive impairment (MCI) patients with an AD-like CSF profile (i.e., A+/T +) (Jack et al., 2018); and tracking the neurodegeneration throughout the AD continuum. With the purpose to constrain and optimize EEG analysis by capitalizing on the high spatial resolution of MRI, we further applied a new model of functional MRI (fMRI)-driven EEG cortical source reconstruction and subsequently tested its advantage in terms of AD diagnostic accuracy.

2. Materials and methods

2.1. Participants

Thirty-nine patients diagnosed with probable AD dementia (ADD) (McKhann et al., 2011) and 86 subjects with amnestic MCI (Albert et al., 2011) were consecutively recruited at the Neurology Unit, IRCCS San Raffaele Scientific Institute (Milan, Italy). Diagnoses were based on an extensive clinical-instrumental evaluation, which included medical history collection, physical and neurological examination, complete neuropsychological evaluation, routine lab, structural neuroimaging assessment, brain FDG-PET, and lumbar puncture for CSF biomarkers dosage (Aβ42, tTau, pTau). Patients showing relevant psychiatric disorders (including major depression), presence of extensive cerebrovascular disease on routine structural brain images, clinical signs or symptoms suggestive for neurodegenerative disorders other than AD, or history of epilepsy were excluded.

According to the new National Institute on Aging and Alzheimer's Association (NIA-AA) research framework, AD should be diagnosed when both markers of amyloidopathy and tauopathy are pathologically altered (Jack et al., 2018). CSF pTau/Aß42 ratio offers the opportunity to consider both markers jointly. As previously described (Santangelo et al., 2019), a ratio $\geq$ 0.13 predicts AD pathology with higher diagnostic accuracy than CSF biomarkers taken singularly. In light of this finding, we classified 51 out of 86 MCI patients as MCI due to AD based on their positive CSF ratio (MCIpos) and 35 as negative cases (MCIneg). Moreover, consistently with the clinical diagnosis, all ADD patients showed a positive ratio (i.e., $\geq$ 0.13).

As part of the research protocol, a 19-channel RS-EEG was acquired for all patients at baseline, whereas resting-state fMRI (RS-fMRI) was available for all ADD patients and for 37 out of 86 MCI (22 MCIpos and 15 MCIneg) subjects.

EEG and fMRI groups of patients were comparable in terms of demographic and clinical data (Table 1 and Supplemental Table 1) and in terms of neuropsychological performances (Supplemental Tables 2 and 3). Among study subjects, the most common chronic pathologies were diabetes type 2 and hypertension, both well controlled by medical therapy. No patient had liver or kidney insufficiency.

Two different groups of age- and sex-matched healthy controls were also recruited for RS-EEG (33 subjects) and RS-fMRI (53 subjects) analysis among friends and spouses of patients and by word of mouth, having no history of cognitive impairment or any other neurological diseases. A complete neuropsychological battery was obtained for fMRI control group, whereas only a Mini-Mental State Examination (MMSE) (Folstein et al., 1975) was administered to the EEG controls. No lumbar puncture was performed in healthy controls.

Supplemental Information displays further details on CSF acquisition and analysis and on neuropsychological assessments.

2.2. EEG and MRI acquisition protocols and pre-processing

19-channel RS-EEGs were recorded for each participant. Using a 3 T MR scanner, T1-weighted, T2-weighted, fluid-attenuated inversion recovery, and RS-fMRI sequences were obtained. RS-fMRI and RS-EEG acquisition protocols and pre-processing have been previously described (Caso et al., 2012; Filippi et al., 2020) and are reported in Supplemental Information. Experienced observers, blinded to patients' identity, performed both analyses.

2.3. Aim 1. Profiling of the EEG patterns

The first goal of this study was to assess EEG patterns in order to characterize patients belonging to the AD continuum (Fig. 1-AIM1).

Current Source Density Analysis. Estimating the current sources from activity recorded with electrodes is an ill-posed inverse problem, since the number of unknown parameters is greater than the number of known parameters. For this purpose we used eLORETA (Pascual-Marqui et al., 2011; Pascual-Marqui, 2007a), which assesses current densities at 6239 voxels with zero error localization within the cortical grey matter (GM) of a realistic head model co-registered to the MNI and Talairach human brain atlases. As previously described (Caso et al., 2012) and reported in Supplemental Information, EEG inverse solutions were estimated within 7 frequency bands (Fig. 1B.1) and subsequently averaged for all voxels belonging to each lobe of interest (frontal, central, parietal, temporal and occipital) by means of a home-made Matlab routine. Differences in ranked eLORETA solutions among subject groups were computed applying age-, sex- and education-adjusted ANOVA models, followed by post-hoc pairwise comparisons (Bonferroni-corrected for multiple comparisons, $p < 0.05$, SPSS version 23.0). The two frequencies with most characteristic patterns of differentiation of study groups were then identified. In order to reduce data amount, subsequent analyses in Aim 2

Table 1
Demographic, clinical and biomarker characteristics according to diagnostic group within the RS-EEG analysis.

	HC	ADD	MCIpos	MCIneg	p ADD *vs* HC	p MCIpos *vs* HC	p MCIneg *vs* HC	p ADD *vs* MCIpos	p ADD *vs* MCIneg	p MCIpos *vs* MCIneg
N	33	39	51	35	–	–	–	–	–	–
Age [years]	66.72 ± 1.17 (49.01–79.74)	68.59 ± 1.10 (55.18–81.67)	72.30 ± 0.73 (61.34–83.62)	71.45 ± 1.16 (55.36–83.50)	1.00	<0.001	0.02	0.02	0.33	1.00
Sex [women/men]	15/18	21/18	30/21	10/25	0.47	0.23	0.14	0.06	0.03	0.06
Education [years]	9.58 ± 0.70 (5.00–21.00)	8.97 ± 0.70 (2.00–18.00)	9.59 ± 0.60 (1.00–18.00)	11.11 ± 0.80 (1.00–23.00)	1.00	1.00	0.96	1.00	0.25	0.74
Disease duration [months]	–	35.38 ± 2.34 (7.03–72.06)	32.93 ± 3.04 (6.05–108.09)	39.45 ± 3.95 (12.00–108.05)	–	–	–	1.00	1.00	0.44
Aβ42 [ng/ml]	–	341.70 ± 20.10 (98.00–572.00)	383.10 ± 14.70 (204.00–663.00)	738.50 ± 40.30 (202.00–1354.00)	–	–	–	0.67	<0.001	<0.001
tTau [ng/ml]	–	559.30 ± 49.30 (199.00–1389.00)	467.30 ± 26.60 (200.00–899.00)	235.90 ± 18.70 (69.00–600.00)	–	–	–	0.15	<0.001	<0.001
pTau [ng/ml]	–	94.53 ± 6.49 (44.00–229.00)	86.08 ± 3.67 (41.00–163.00)	49.68 ± 3.17 (19.00–87.00)	–	–	–	0.55	<0.001	<0.001
pTau/Aβ42	–	0.29 ± 0.02 (0.14–0.75)	0.24 ± 0.01 (0.13–0.45)	0.07 ± 0.01 (0.04–0.12)	–	–	–	0.03	<0.001	<0.001
ADL	–	69.69 ± 5.11 (0.00–100.00)	97.00 ± 0.91 (83.34–100.00)	99.02 ± 0.68 (83.34–100.00)	–	–	–	<0.001	<0.001	0.89
IADL	–	90.17 ± 4.05 (0.00–100.00)	92.74 ± 2.07 (50.00–100.00)	92.66 ± 2.34 (50.00–100.00)	–	–	–	1.00	1.00	1.00
CDRsb	–	3.47 ± 0.51 (0.50–12.00)	1.19 ± 0.22 (0.50–7.50)	1.80 ± 0.21 (0.50–4.50)	–	–	–	0.49	0.61	1.00
MMSE	27.61 ± 0.33 (21.00–30.00)	19.46 ± 0.83 (5.00–28.00)	25.82 ± 0.34 (21.00–30.00)	26.54 ± 0.38 (20.00–30.00)	<0.001	0.02	0.03	<0.001	<0.001	1.00

Values are means ± standard errors (range). Differences of ranked transformed values were assessed through ANOVA models followed by post-hoc pairwise comparisons (Bonferroni-corrected for multiple comparisons, $p < 0.05$, SPSS). Abbreviations: Aβ42 = amyloidogenic beta amyloid, ADD = Alzheimer's disease dementia, ADL = activities of daily living, CDRsb = clinical dementia rating scale sum of boxes, HC = healthy controls, IADL = instrumental activities of daily living, MCI = mild cognitive impairment (pos = pTau/Aβ42 ≥ 0.13, neg = pTau/ Aβ42 < 0.13), MMSE = Mini-Mental State Examination, pTau = CSF phosphorylated Tau, tTau = CSF total Tau.

were focused only on these two frequencies.

2.4. Aim 2. fMRI network-driven analysis of RS-EEG data

One of the main goals of the present study was to evaluate how the integration of RS-fMRI ameliorates, by constraining the analysis of electrophysiological signals, RS-EEG discrimination among groups. With this purpose, the following EEG analyses were driven by the previous selection of the two frequency bands (Fig. 1B.1) and by fMRI networks identified with Independent Component Analysis (ICA) (Fig. 1A.1).

Regional correspondence between MRI and RS-EEG data. MRI GM was parcellated into 220 similarly-sized brain regions of interest (ROIs), which included cerebral cortex and basal ganglia but excluded the cerebellum. The methodological process has been recently described (Filippi et al., 2020). Subsequently, using MNI coordinates, the exact correspondence of each voxel of eLORETA brain head model with the 220 MRI brain regions was obtained.

Definition of fMRI networks (Independent Component Analysis). The most informative fMRI networks were identified with ICA (Canu et al., 2017). Specifically, we applied Independent Component Analysis-based Automatic Removal of Motion Artifacts (ICA-AROMA) on pre-processed RS-fMRI data in order to identify those independent components (ICs) representing motion-related artifacts (McKhann et al., 2011). This method calculates a set of spatial and temporal discriminative features and a classification procedure identifies ICs representing motion artifacts. In particular, the spatial overlap of each component with the edges of brain and CSF is evaluated, as well as the frequency content and the temporal correlation with realignment parameters of the IC time-series. ICs classified as motion-related were removed from the fMRI dataset by means of linear regression. Resulting fMRI dataset was then high-pass filtered (cut-off frequency of 0.01 Hz) and co-registered to the participant's 3D T1-weighted image using affine boundary-based registration as implemented in FLIRT (Albert et al., 2011; Mazzeo et al., 2016). Subsequently, the fMRI data were transformed to the MNI152 standard space with 4 mm isotropic resolution using non-linear registration through FNIRT. The final fMRI data, containing 196 time-points for each subject, were temporally concatenated across subjects to create a single 4D dataset. This fMRI dataset was then decomposed into ICs with a free estimation for the number of components using Multivariate Exploratory Linear Optimized Decomposition into Independent Components (MELODIC) (Beckmann et al., 2005). In order to identify the subject-specific temporal dynamics and spatial maps associated with each group IC, a dual regression analysis was applied. Among group-IC spatial maps, ICs of interest (default mode network, primary visual, right fronto-parietal and visual-associative networks) were selected by visual inspection based on previous literature (Smith and Nichols, 2009). To be confident with the visual inspection, fMRI networks were also spatially correlated to the Shirer functional networks (Shirer et al., 2012). This analysis was performed in order to identify the most similar ICs to the different networks. Then, a dual-regression procedure was performed, which involves: (i) the use of the selected group-IC spatial maps in a linear model fit (spatial regression) against the single subject fMRI data sets, resulting in matrices describing temporal dynamics for each IC and subject; and (ii) the use of these time-course matrices which are entered into a linear model fit (temporal regression) against the associated fMRI data set to estimate subject-specific spatial maps. Altered connectivity within the selected fMRI networks was identified in the ADD group compared with healthy controls using age-, sex-, education- and GM-adjusted ANOVA models, followed by a nonparametric permutation tests (5000 permutations, $p < 0.05$) (Fig. 1A.1). Only networks showing an alteration of connectivity were selected for subsequent EEG analysis. Brain regions (i.e., selected from the abovementioned 220 ROIs) included for more than 50% of

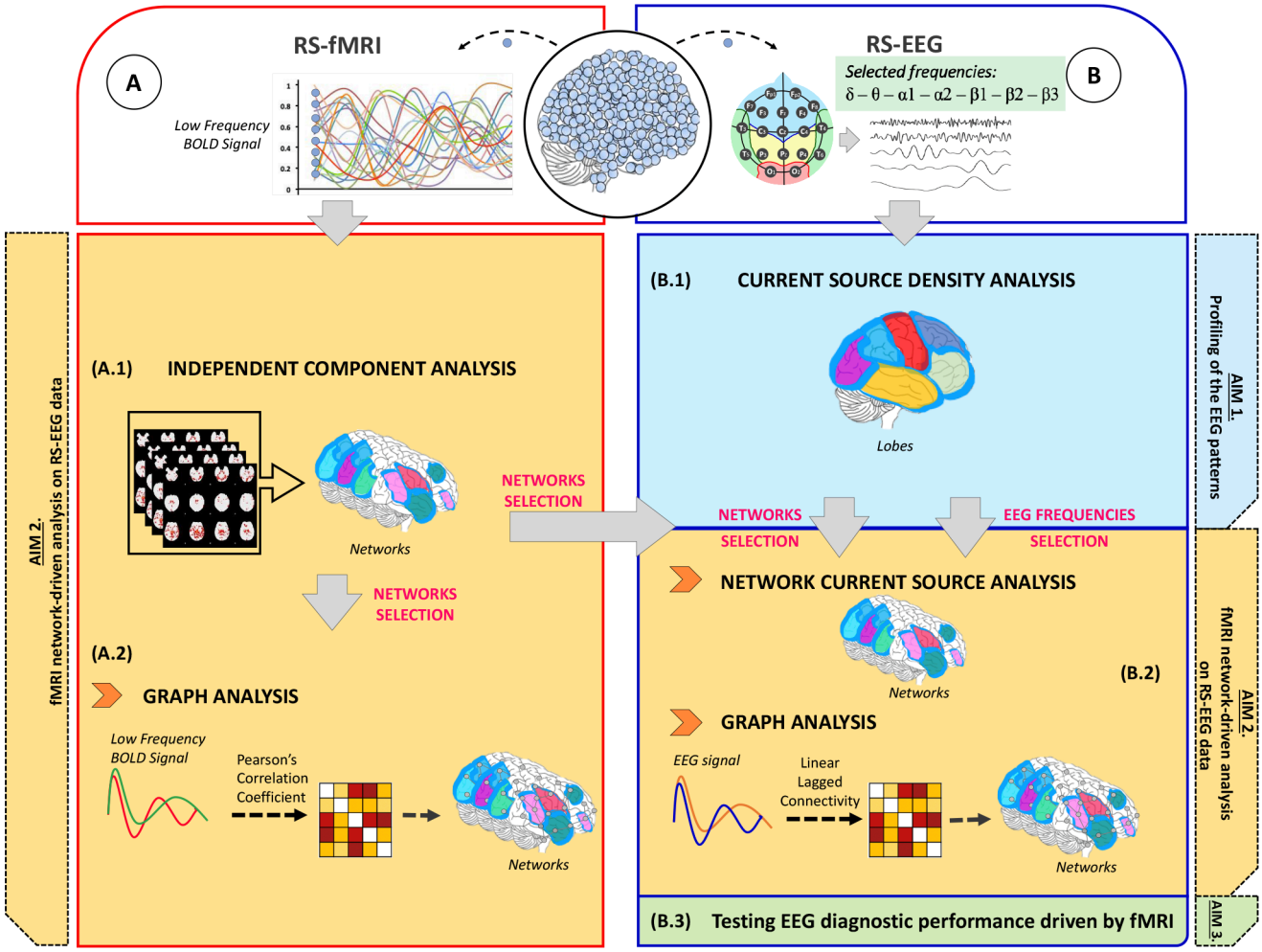

Fig. 1. RS-fMRI and EEG analysis pipeline. Preprocessing of RS-fMRI data (A) and RS-EEG data (B) were applied for patient groups and healthy controls. To delineate EEG patterns within the AD continuum (AIM 1), current source density analysis was computed on EEG data (B.1) identifying the most informative frequency bands. Subsequently, fMRI-driven analysis was performed on RS-EEG data (AIM 2). Firstly, independent component analysis was performed on fMRI data (A.1) in order to select the most informative functional networks. Subsequently, network current source analysis was applied on RS-EEG data within the selected networks and frequencies (B.2). Furthermore, RS-fMRI and EEG graph theoretical analyses were performed only within the fMRI networks (A.2) and frequency bands (only for EEG analysis) (B.2). AIM 3: EEG Diagnostic performance driven by fMRI was tested (B.3). Abbreviations: BOLD = blood-oxygen-level-dependent; RS-EEG = resting-state electroencephalogram; RS-fMRI = resting-state functional magnetic resonance imaging.

their volume into the fMRI ICA-based networks (Supplemental Table 4) were then considered as 'ICA-regions' in the EEG ICA-based network current source analysis and in the EEG and fMRI ICA-based network graph analysis.

EEG ICA-based network current source analysis. eLORETA values for the two selected frequencies (see Aim 1) were extracted from voxels belonging to the ICA-regions. All voxel values were compared among groups using age-, sex- and education-adjusted ANOVA models (FDR-corrected, $p < 0.05$, SPSS version 23.0) (Fig. 1B.2). The percentage of statistically significant voxels was calculated per each network.

EEG and fMRI ICA-based network graph analysis. EEG and fMRI graph analysis were performed considering only ICA-regions in all study subjects. Initially, concerning EEG graph analysis, Linear Lagged Connectivity (LLC) was computed considering the 220 ROIs in patient groups and matched healthy controls (Fig. 1B.2) (Pascual-Marqui et al., 2011; Pascual-Marqui, 2007b). For the functional brain network construction undirected, weighted graphs were obtained by computing LLC at the two selected frequency bands. In particular, mean multivariate time series were extracted from the 220 ROIs by averaging the signal from all voxels within each region (see Supplemental Information). Concurrently, undirected, weighted graphs describing fMRI connectivity were also obtained in patient groups and matched healthy controls, considering the 220 ROIs; the methodological approach has been recently described (Fig. 1A.2) (Filippi et al., 2020).

Basal ganglia ROIs were excluded from the analysis because of the lack of correspondence between fMRI and EEG data. Moreover, to avoid considering spurious functional connections, EEG and fMRI functional interactions were required to be present in a structural connectivity matrix of an independent healthy control sample (N = 90, mean age 62.3 ± 8.07 years, 51 women/39 men), i.e., we measured functional interactions only where an anatomical connection between two areas occurs in the independent healthy control sample, as recently described (Filippi et al., 2020). These healthy controls were considered only for the construction of the structural architecture (Filippi et al., 2020).

Topographical metrics, including nodal strength, characteristic path length, local efficiency and clustering coefficient were then explored using the Brain Connectivity Matlab toolbox (http://www.brain-connectivity-toolbox.net) only within ICA-regions (Fig. 1A.2 and 1B.2) (Sporns et al., 2004). All the remaining ROIs considered in the LLC and fMRI matrices were excluded from further analysis. Rank-transformed metrics were then compared between groups using age-, sex- and education-adjusted ANOVA models, followed by post-hoc pairwise comparisons, Bonferroni-corrected for multiple comparisons ($p < 0.05$, SPSS version 23.0).

2.5. Aim 3. Testing EEG diagnostic performance driven by fMRI

To investigate the advantage of fMRI network-driven RS-EEG source analysis in distinguishing MCIpos from MCIneg patients, binomial logistic regression models were computed for the frequency band with lobar highest statistical power of differentiation, both at lobar and at ICA-based network level, and accuracy of each model was calculated (SPSS version 23.0) (Fig. 1B.3). Specifically, the belonging to either MCIpos or MCIneg group was introduced as dependent variable in the models, whereas current density values within each lobe or ICA-based network were singularly implemented as predictive variable, together with age, sex and education. Receiver operating characteristic (ROC) curves for lobar and fMRI ICA-based network prediction models were subsequently built, and accuracy, sensitivity and specificity were calculated. Finally, in order to compare the performance of EEG alone (i.e., at lobar level) and driven by fMRI (i.e., at ICA-based network level), we used the single-tailed Hanley-McNeil area under the curve (AUC) test (Hanley and McNeil, 1983).

3. Results

3.1. Aim 1. Profiling of the EEG patterns

ADD vs other groups. After current source analysis, ADD patients showed higher delta density in central, parietal and occipital lobes relative to both MCI groups and controls, and in temporal lobes in comparison to healthy and MCIneg subjects (Fig. 2A). Similarly, ADD showed an increased current density in the theta band within all lobes when compared to controls, and in central, parietal and occipital regions in comparison to MCIneg subjects, whereas no differences were found when compared to MCIpos patients. Moreover, in ADD patients, alpha1 density appeared decreased in all lobes relative to MCIpos subjects, and in temporal and occipital regions when compared to controls. Conversely, a diffuse lower alpha2 current density was detected in ADD relatively to all other groups. Density at beta1 resulted significantly lower in parietal and occipital lobes in ADD when compared to MCIneg subjects and controls. Finally, occipital beta2 density was lower in ADD than in healthy subjects.

MCIpos vs MCIneg. MCIpos patients showed greater theta density in central, parietal, temporal and occipital lobes relative to MCIneg subjects (Fig. 2A).

MCIpos vs healthy controls. MCIpos patients showed a significantly greater theta density in all lobes (Fig. 2A). They also showed lower beta2 density in parietal and occipital lobes.

MCIneg vs healthy controls. The analysis revealed no significant differences (Fig. 2A).

3.2. Aim 2. fMRI network-driven analysis of RS-EEG data

Since theta band could diffusely differentiate MCIpos from MCIneg

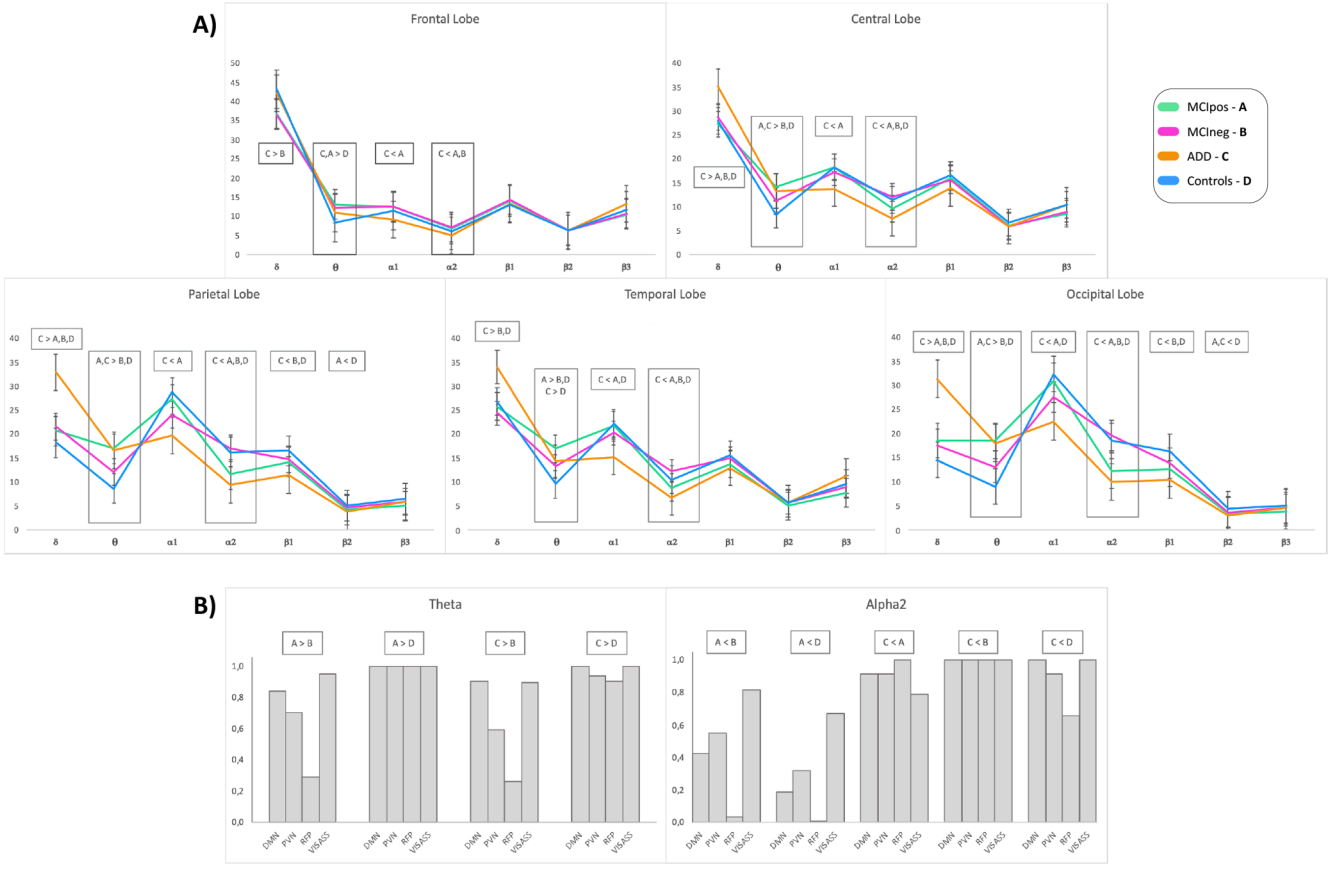

Fig. 2. Lobar (A) and network (B) current source density analysis on EEG data. A) Mean values of lobar current density at the different frequencies are reported for MCIpos (A), MCIneg (B), ADD (C) and controls (D). Significant comparisons reported in the boxes are referred to age-, sex- and education-adjusted ANOVA models of rank transformed values, followed by post-hoc pairwise comparisons (Bonferroni-corrected for multiple comparisons, p value < 0.05). Error bars are shown. Lengthened boxes mark the two selected frequencies for the subsequent EEG analysis. B) Percentage of voxels within each selected RS-fMRI network. Only comparisons showing significant differences in at least one network are reported per each freuency band (p value < 0.05). P value refers to age-, sex- and education-adjusted ANOVA models (FDR-corrected, $p < 0.05$) of rank transformed values. Abbreviations: ADD = Alzheimer's disease dementia; DMN = default mode network; MCIneg = Mild cognitive impairment with pTau/Aß42 < 0.13; MCIpos = Mild cognitive impairment with pTau/Aß42 ≥ 0.13; PVN = primary visual network; RFP = right frontal-parietal network; VISASS = visual-associative network.

patients, and alpha2 band distinguished ADD from all other groups in all lobes, both frequencies were considered for subsequent analyses in Aim 2 (Fig. 2A). Furthermore, with regards to the selection of fMRI networks, ICA was performed. A decreased fMRI connectivity in ADD patients relative to controls was detected within the four networks, including only posterior regions of the brain. The default-mode network (DMN) showed an alteration of connectivity in the left posterior cingulate cortex, in the right midcingulate cortex, in the left angular cortex, as well as in the middle temporal gyrus and in the precuneus, bilaterally; anterior regions of DMN were instead mainly spared. The connectivity within the right frontal-parietal network (RFP) was mainly altered in the right middle occipital gyrus and cuneus, as well as in right inferior parietal gyrus and angular gyrus; also in this case, anterior regions of this network appeared substantially preserved. A reduced connectivity was found also in the primary visual network (PVN) within the lingual and the calcarine cortex bilaterally, within the right occipital and temporal middle gyri and the left fusiform gyrus. Finally, the visual-associative network (VISASS) was affected within the calcarine cortex bilaterally, the right lingual gyrus and the bilateral middle and inferior occipital and fusiform gyri (Fig. 3).

ADD vs other groups. Source analysis within fMRI ICA-based networks showed a widespread significant increase in theta density in ADD patients compared to healthy controls, in 100% of DMN (932/932 voxels), in 94% of PVN (701/742 voxels), in 89.9% of RFP (841/935 voxels) and in 100% of VISASS (554/554 voxels). Theta frequency band also differentiated ADD from MCIneg patients in 90.2% of DMN, in 58% of PVN, in 26.2% of RFP and in 89.9% of VISASS, whereas no differences were found when comparing ADD and MCIpos patients. The analysis also showed a lower alpha2 density in ADD patients than in healthy subjects (DMN: 100%, PVN: 91%, RFP: 65.2%, VISASS: 100%), MCIpos patients (DMN: 90.7%, PVN: 91.5%, RFP: 99.6%, VISASS: 78.7%), and MCIneg patients (100% of all four networks analyzed) (Fig. 2B).

EEG ICA-based network graph analysis in theta band showed a higher nodal strength, local efficiency and clustering coefficient, in addition to a shorter path length, in ADD patients when compared to controls in DMN, PVN and VISASS (Fig. 4 and Supplemental Table 5). Similar results were obtained (including also RFP) when considering the ADD *vs* MCIneg comparison. No differences were detected between ADD and MCIpos patients. Regarding alpha2 frequency band, the analysis revealed a lower nodal strength and clustering coefficient in RFP network of ADD patients compared with controls (Fig. 4 and Supplemental Table 5), whereas the comparison with MCIneg and MCIpos patients showed no significant differences. Furthermore, graph analysis of RS-fMRI data showed similarly less well-ordered brain networks in

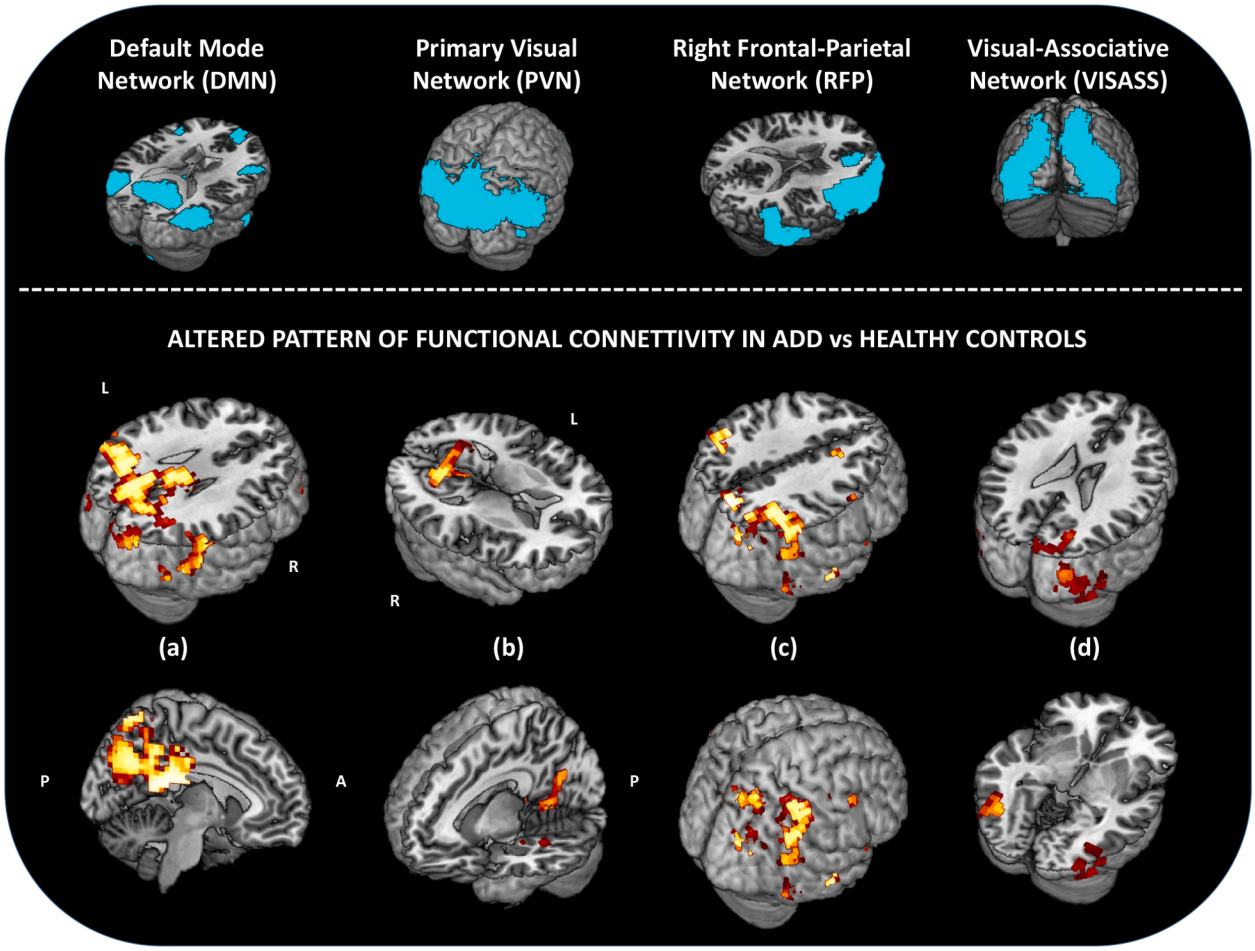

Fig. 3. Independent Component Analysis (ICA) showing decreased functional connectivity in Alzheimer's disease dementia patients compared with controls. First line shows the selected fMRI ICA-based networks (highlighted in light blue). Second and third lines report three dimensional rendered brains illustrating altered patterns of functional connectivity in Alzheimer's disease dementia (ADD) patients compared with controls ($p < 0.05$ FDR-corrected) within networks: a) default mode network (left posterior cingulate cortex, right midcingulate cortex, left angular cortex and middle temporal gyrus and precuneus bilaterally), b) primary visual network (lingual and calcarine cortex bilaterally, right occipital and temporal middle gyrus and left fusiform gyrus), c) right frontal-parietal network (right middle occipital gyrus and cuneus, so as in right inferior parietal gyrus and angular gyrus) and d) visual associative network (calcarine cortex bilaterally, right lingual gyrus and bilateral middle and inferior occipital gyri and bilateral fusiform gyri). (For interpretation of the references to colour in this figure legend, the reader is referred to the web version of this article.)

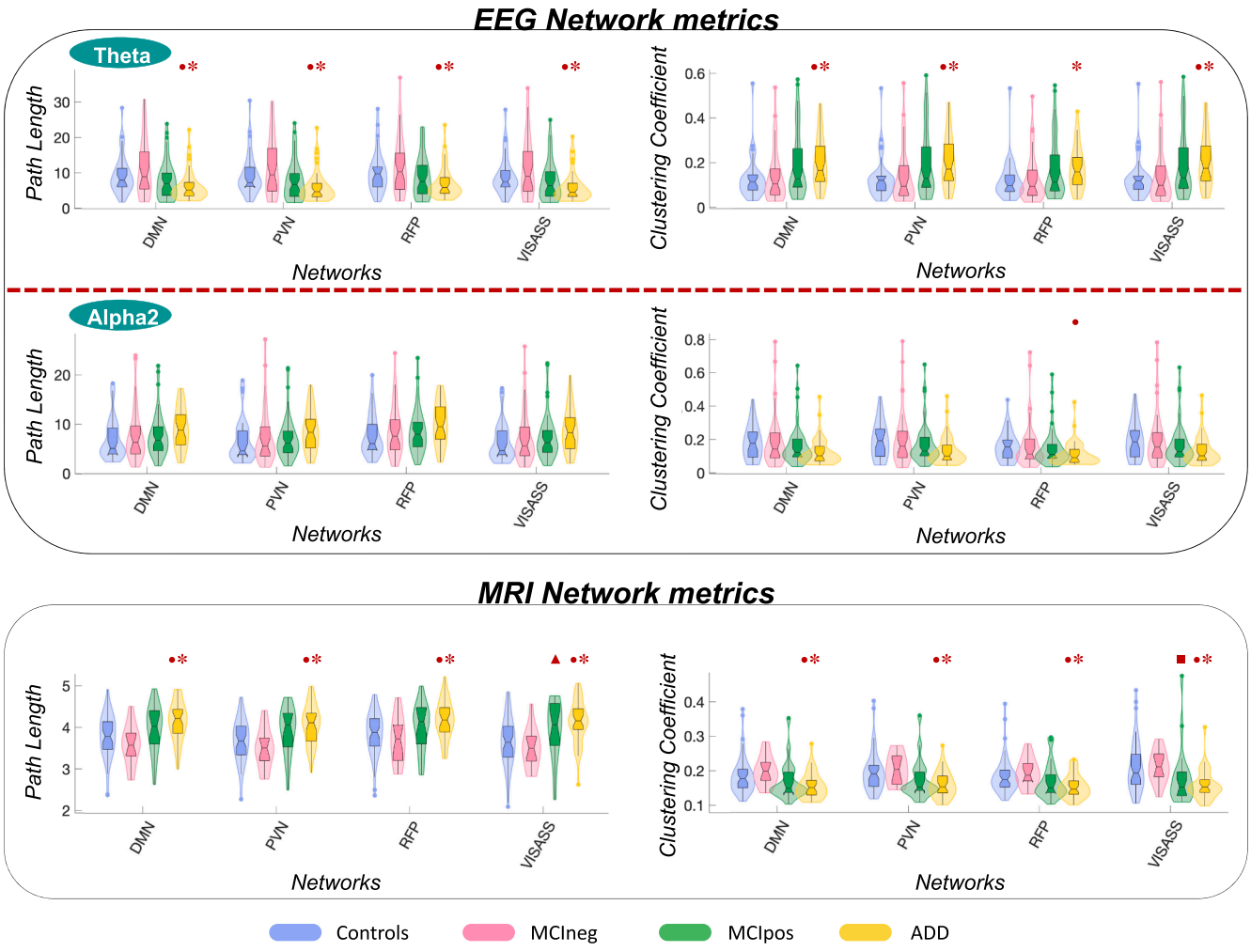

Fig. 4. RS-fMRI and EEG graph analysis properties within fMRI networks. Violin plots of clustering coefficient and path length of selected networks (the two most significant metrics) are shown for patient groups and healthy controls. Both graph metrics were calculated based on the Linear Lagged Connectivity for alpha2 and theta frequency bands from RS-EEG data (on the top of the figure) and based on Pearson's Correlation Coefficient from RS-fMRI data (on the bottom of the figure). Boxplots are reported within violin plots. The horizontal lines in each box plot represents, from the bottom to the top, the 25th percentile, the median and 75th percentile. Whiskers represent the minimum and maximum values. All the dots outside the confidence interval are considered as outliers. Significant comparisons are reported (p values < 0.05). P values refer to age, sex and education-adjusted ANOVA models of rank transformed values, followed by post-hoc pairwise comparisons (Bonferroni-corrected for multiple comparisons). ●: ADD *vs* Controls; *: ADD *vs* MCIneg; ■: MCIpos *vs* Controls; ▲: MCIpos *vs* MCIneg. Abbreviations: ADD = Alzheimer's disease dementia, DMN = default mode network, MCI = mild cognitive impairment (pos = pTau/Aß42 $\geq$ 0.13, neg = pTau/Aß42 $<$ 0.13), PVN = primary visual network, RFP = right frontal-parietal network, VISASS = visual-associative network.

ADD subjects when compared with both controls and MCIneg patients, exhibiting alterations in DMN, PVN, RFP and VISASS (lower nodal strength, local efficiency and clustering coefficient and longer path length).

MCIpos vs MCIneg. Source analysis showed a significant greater theta density in MCIpos in 83.6% of DMN, in 69.8% of PVN, in 29.2% of RFP and in 95.3% of VISASS (Fig. 2B). Within the alpha2 band, MCIpos subjects showed lower current density in 42% of DMN, 54.9% of PVN, in 30 voxels out of 935 in RFP and in 81.6% of VISASS.

EEG ICA-based network graph analysis showed no statistical differences between MCIpos and MCIneg in the two selected frequencies (Fig. 4 and Supplemental Table 5). On RS-fMRI graph analysis, MCIpos subjects showed longer path length within VISASS relative to MCIneg.

MCIpos vs healthy controls. eLORETA source analysis within selected fMRI networks showed a significant greater theta current density in MCIpos in 100% of DMN, PVN, RFP and VISASS (Fig. 2B). In addition, lower alpha2 density was found only in VISASS (66.7%).

EEG ICA-based network graph analysis showed no statistical differences between the two groups at theta and alpha2 frequency bands (Fig. 4 and Supplemental Table 5). Concerning RS-fMRI graph analysis, MCIpos patients showed lower nodal strength, local efficiency and clustering coefficient only within the VISASS. Moreover, a lower local efficiency was found in MCIpos within the DMN relative to controls.

MCIneg vs healthy controls. No significant differences were found by source analysis and EEG and RS-fMRI graph analysis (Fig. 2B, Fig. 4 and Supplemental Table 5).

3.3. Aim 3. Testing EEG diagnostic performance driven by fMRI

MCIpos were differentiated from MCIneg patients at lobar level by theta band only. Therefore, Aim 3 analysis was performed at this frequency band. Table 2 shows accuracy, sensitivity and specificity obtained from the ROC-curve analysis applied to lobes and ICA-based networks. Accuracy was over the acceptance level of 70% in all cases. After the application of Hanley-McNeil AUC test no statistically significant differences were found (p-value = 0.17).

4. Discussion

Our study explored the accuracy of RS-EEG-based biomarkers in the

Table 2
Accuracy, Sensitivity and Specificity of EEG current source analysis at lobar and network level.

Comparison	Frequency band	Lobes/ Networks	Accuracy	Sensitivity	Specificity
MCIpos *vs* MCIneg	Theta	Central	75.40%	71.40%	70.60%
		Parietal	75.70%	71.40%	70.60%
		Temporal	74.50%	71.40%	70.60%
		Occipital	75.80%	71.40%	70.60%
		DMN	76.80%	71.40%	70.60%
		PVN	76.60%	74.30%	70.60%
		RFP	75.80%	71.40%	70.60%
		VISASS	76.60%	74.30%	68.60%

Values are reported as Accuracy, Sensitivity and Specificity calculated on receiver operating characteristic curves (comprehensive of age, sex and education). Abbreviations: DMN = Default Mode Network, MCI = mild cognitive impairment (pos = pTau/ Aβ42 $\geq$ 0.13, neg = pTau/Aβ42 < 0.13), PVN = Primary Visual Network, RFP = Right Frontal-Parietal Network, VISASS = Visual-Associative Network.

early diagnosis of AD and in tracking the progression of neurodegeneration throughout the AD continuum. Many aspects support the usefulness of EEG recordings in the study of AD patients: non-invasiveness, speed of execution, low cost and large availability. Moreover, acquisition in resting-state conditions does not require external stimuli and necessitates therefore only minimal compliance. With the intent of exploiting MRI high spatial resolution and optimizing EEG analysis, we further developed a novel fMRI-driven EEG source reconstruction model. By applying ICA on fMRI data, resting-state networks showing altered functional connectivity in our ADD sample were identified, and corresponding eLORETA inverse solutions were then computed and extracted. To our knowledge, in the recent scenario of fMRI-driven EEG analysis for the study of brain function, our model is unique (Jorge et al., 2014).

The comparison of eLORETA solutions at lobar level confirmed the trend towards a general slowing of oscillatory neural activity as a consequence of AD pathology (Caso et al., 2012; Babiloni et al., 2016; Jovicich et al., 2019). Even years before clinical symptoms appear, indeed, amyloid and tau deposition affects synaptic function (de Wilde et al., 2016), determining a progressive disruption of inter-neuronal connections and a subsequent slowing of oscillatory activity (D'Amelio and Rossini, 2012). Our analysis of lobar EEG cortical sources, in particular, suggests that theta band may be consistently altered already in the prodromal phases of AD clinical syndrome, thus emerging as early hallmark of AD pathology. We observed indeed that both MCIpos and ADD patients shared a widespread and comparable increase in theta density relative to both MCIneg and healthy controls (Fig. 2A). On the contrary, MCIpos and ADD subjects were characterized by a decrease in beta2 density when compared to healthy controls, even if limited to the occipital lobe (Fig. 2A). ADD, but not MCIpos, was further associated with a widespread augmentation of delta power, reasonably stemming from a longer duration of the disease (Babiloni et al., 2013). The rare previous studies focusing on profiling EEG activity in AD and its relationship with CSF biomarkers seem to corroborate our findings in theta band; decreased Aß42 has been shown to significantly correlate with theta global field power (i.e., a measure of global strength of scalp potential fields) in a population of mild AD and MCI patients (Smailovic et al., 2018), and with the logarithms of theta current density over the temporal regions in AD subjects (Hata et al., 2017).

The current source analysis at lobar level also outlined in ADD patients a widespread reduction of alpha2 current density, hallmark of resting-state wakefulness (Laufs et al., 2003) and underlying several cognitive functions (namely, attentive and mnestic skills) (Schurmann and Basar, 2001; Stam et al., 1999). This finding is in line with previous reports (Gianotti et al., 2007; Babiloni et al., 2013; Choi et al., 2019). Looking at Fig. 2A, furthermore, it is possible to appreciate a visual trend of progressive alteration of alpha2 power density over the posterior regions among patient groups belonging to the AD continuum (ADD < MCIpos < healthy controls), suggesting novel insights into the pathophysiological meaning of alpha2 band.

The ICA applied to fMRI data in ADD compared to healthy subjects, revealed an alteration of fMRI connectivity mostly confined in posterior regions in all the networks (Fig. 3), quite preserving anterior regions of DMN and RFP, consistently with previous literature (Canu et al., 2017; Jovicich et al., 2019; Zhou et al., 2017; Agosta et al., 2014; Zhang et al., 2010; Xie and He, 2011).

Subsequent EEG analysis of current sources extracted from fMRI ICA-based networks corroborated theta discriminative nature of AD pathology, regardless of severity stage (Fig. 2B). ADD and MCIpos patients, indeed, showed a higher theta current density than both MCIneg and healthy subjects. Consistently with the results of the ICA applied to fMRI data, results of both lobar and ICA-based network eLORETA analyses seem to indicate that the major disruption of electrical sources lays in the posterior regions of the brain, typically more involved by AD pathology since its initial stages; the widest theta alteration in MCIpos patients with respect to MCIneg and healthy subjects was indeed observed in parietal and occipital lobes and in VISASS and DMN (Fig. 2), which mainly extend within parietal, occipital and temporal regions (Supplemental Table 4). On the contrary, either none or minimal differences were found in frontal lobes and in RFP when comparing MCIneg with ADD and MCIpos patients. This seems to be driven by two factors: first, the increase of theta density was relatively modest in frontal regions of patients with AD (both MCI and ADD) (Fig. 2A); secondly, MCIneg subjects showed an increase in theta density in the anterior regions, comparable to that of patients with AD (Fig. 2A). Consistently, MCIpos patients were slightly (i.e., non-significantly) more impaired in 'posterior' cognitive functions (i.e., mnestic and visuo-spatial skills) than MCIneg subjects, whereas frontal (i.e., attentive and executive) skills of two MCI groups substantially overlap (Supplemental Table 2). On the contrary, the lack of difference in theta density between ADD and MCIpos groups despite their differences in cognitive performances seems to confirm that theta alteration might develop early during AD pathology and that it should be considered a marker of pathology, rather than of disease progression.

Moreover, the fMRI-driven analysis revealed that the alpha2 band could significantly differentiate ADD from MCIpos patients and MCIpos from healthy subjects, confirming its potential role as a neurodegeneration biomarker of AD pathology, only visually guessed at lobar level (Fig. 2). Consistently, one of the abovementioned studies, which analyzed the relationship between EEG activity and CSF biomarkers in AD patients (Hata et al., 2017), showed a negative correlation between source connectivity in alpha2 band in the right posterior temporal regions and the CSF tTau level, recently included in the class of neurodegeneration biomarkers (Jack et al., 2018). However, a clarification must be done; looking at Fig. 2A, it can be appreciated how in frontal lobes MCIpos patients showed a greater difference from ADD patients than healthy subjects did. Concurrently, in Fig. 2B, significant differences in RFP were wider in the MCIpos *vs* ADD comparison than in the healthy controls *vs* ADD one. We can speculate that this finding might be at least partially justified by the "anteriorization" of alpha electrical field due to AD pathology described in previous studies (Smailovic and Jelic, 2019), which could result in a transient augmentation of alpha2 sources within frontal regions in prodromal phases of AD. In support of this hypothesis, Fig. 2B clearly shows that the largest alpha2 decrease when comparing MCIpos patients with MCIneg and with healthy subjects was found within VISASS and PVN, both extending within posterior regions (i.e., where, in normal condition, the strongest sources of alpha frequency band lay) (Smailovic and Jelic, 2019).

Moving to graph analysis applied to fMRI-driven eLORETA solutions in theta band, ADD patients showed a significant higher degree of apparent network efficiency (i.e., higher segregation metrics and shorter path length) when compared to both controls and MCIneg patients (Fig. 4 and Supplemental Table 5). The same phenomenon was true for

MCIpos subjects, yet not meeting full statistical significance, probably due to greater value variance. These findings sound counterintuitive; however, it is reasonable to assume that the described transition towards more ordered connectivity at theta frequency might be a consequence of the described general slowing of electrical activity due to AD pathology and clinical benefit of such phenomenon should be doubted. Indeed, previous studies that have assessed the EEG complexity of AD patients by both linear and nonlinear approaches found that the EEG of AD patients were more regular than age-matched controls within theta frequency band, which is in line with our findings (Ifeachor E., 2018; Cai et al., 2018).

A widespread alteration of network configuration within ADD patients was also observed in alpha2 band, but with an opposite trend of decreasing segregation metrics and increasing path length. Even if not being fully significant, probably due to the strict statistical process, a visual inspection of Fig. 4 allows moreover to depict MCIpos group as an intermediate stage of alteration between ADD and healthy subjects; this reasonably reflects a progressive transition toward a random reconfiguration of brain connectome in alpha2 frequency (Xie and He, 2011). Future studies with a larger sample and a longitudinal design should lead to the full statistical significance.

Previous EEG studies exploring AD brain connectomics showed discordant results, basically due to different methodological approaches, which complicates the comparability of obtained results (Vecchio et al., 2017; Xie and He, 2011; Lazarou et al., 2020; Tijms et al., 2013). Among others, for instance, one study applied linear lagged coherence to eLORETA solutions extracted from a population of AD, MCI and healthy subjects, describing network reconfiguration profiles which are only partially in line with our findings (Vecchio et al., 2014, 2015); in parallel with an increased normalized clustering coefficient in theta band in MCI and AD patients, indeed, they also described an increased normalized path length. As previously described (Tijms et al., 2013), though, an increased unnormalized path length can be associated with a decreased normalized path, which makes the interpretation of results ambiguous. Further methodological differences (e.g., patient classification and matrices construction) may at least partially account for discordant results.

Moving to RS-fMRI graph analysis, ADD patients showed a severe alteration of graph properties in all considered networks, whereas MCIpos patients were characterized by a less profound connectivity impairment. These findings are in line with a large body of previous literature (Filippi et al., 2020; Agosta et al., 2012; Jones et al., 2016; delEtoile and Adeli, 2017).

Our study has at least two main limitations: first, we recruited two different groups of healthy subjects for fMRI and EEG analysis, which might have led to biases in the analysis, albeit limited. Moreover, controls who entered the EEG analysis did not perform a complete neuropsychological assessment; they underwent nevertheless an accurate medical history collection and a complete neurological examination, which excluded the presence of past or present neurological diseases, together with a MMSE (Folstein et al., 1975), showing significantly higher scores than other study groups.

The identification of early biomarkers of AD pathology that could help distinguish MCI patients in urgent need of therapies is of great interest in the recent scenario. We found that the most accurate EEG biomarker differentiating MCIpos from MCIneg patients was represented by the increase in theta band density, reaching a good diagnostic accuracy (over 70%) both at lobar level (75.8% in occipital lobe) and when the analysis was driven by fMRI ICA-based networks (76.8% in DMN – Table 2). Despite the slight increase in accuracy, though, Hanley-McNeil test did not find a full statistically significant difference between lobar and network AUCs. Concurrently, fMRI-driven EEG analysis allowed highlighting the role of alpha2 band density as neurodegeneration biomarker by correlating it with disease progression. Furthermore, graph analysis applied to both eLORETA solutions and fMRI data showed a characteristic disruption of connectivity measures in patients with AD. Future studies focusing on a greater sample and with a longitudinal design are required to further explore the role of fMRI-driven EEG source estimation analysis in the diagnostic workup of AD pathology.

Funding

This study was partially supported by the Italian Ministry of Health (GR-2011–02351217).

Declaration of interest

G. Cecchetti, S. Basaia, C. Cividini, M. Cursi, R. Santangelo, F. Caso, F. Minicucci, G. Magnani report no disclosures. F. Agosta is Section Editor of *NeuroImage: Clinical*; has received speaker honoraria from Biogen Idec, Roche and Philips; and receives or has received research supports from the Italian Ministry of Health, AriSLA (Fondazione Italiana di Ricerca per la SLA), and the European Research Council. M. Filippi is Editor-in-Chief of the *Journal of Neurology* and Associate Editor of *Human Brain Mapping*; received compensation for consulting services and/or speaking activities from Alexion, Almirall, Bayer, Biogen, Celgene, Eli Lilly, Genzyme, Merck-Serono, Novartis, Roche, Sanofi, Takeda, and Teva Pharmaceutical Industries; and receives research support from Biogen Idec, Merck-Serono, Novartis, Roche, Teva Pharmaceutical Industries, Italian Ministry of Health, Fondazione Italiana Sclerosi Multipla, and ARiSLA (Fondazione Italiana di Ricerca per la SLA).

CRediT authorship contribution statement

Giordano Cecchetti: Conceptualization, Formal analysis, Data curation, Writing - original draft, Writing - review & editing. **Federica Agosta:** Conceptualization, Data curation, Writing - review & editing. **Silvia Basaia:** Conceptualization, Formal analysis, Data curation, Methodology, Writing - original draft. **Camilla Cividini:** Conceptualization, Formal analysis, Data curation, Methodology, Writing - original draft. **Marco Cursi:** Conceptualization, Formal analysis, Data curation, Methodology, Writing - review & editing. **Roberto Santangelo:** Investigation, Writing - review & editing. **Francesca Caso:** Investigation, Writing - review & editing. **Fabio Minicucci:** Investigation, Writing - review & editing. **Giuseppe Magnani:** Investigation, Writing - review & editing. **Massimo Filippi:** Supervision, Resources, Writing - review & editing.

Declaration of Competing Interest

The authors declare that they have no known competing financial interests or personal relationships that could have appeared to influence the work reported in this paper.

Appendix A. Supplementary data

Supplementary data to this article can be found online at https://doi.org/10.1016/j.nicl.2021.102711.

References

Agosta, F., Pievani, M., Geroldi, C., Copetti, M., Frisoni, G.B., Filippi, M., 2012. Resting state fMRI in Alzheimer's disease: Beyond the default mode network. Neurobiol Aging 33, 1564–1578.

Agosta, F., Dalla Libera, D., Spinelli, E.G., et al., 2014. Myeloid microvesicles in cerebrospinal fluid are associated with myelin damage and neuronal loss in mild cognitive impairment and Alzheimer disease. Ann Neurol 76, 813–825.

Albert, M.S., DeKosky, S.T., Dickson, D., et al., 2011. The diagnosis of mild cognitive impairment due to Alzheimer's disease: recommendations from the National Institute on Aging-Alzheimer's Association workgroups on diagnostic guidelines for Alzheimer's disease. Alzheimers Dement 7, 270–279.

Al-Nuaimi, A.J., Sun, E.L., Ifeachor, E., 2018. Complexity Measures for Quantifying Changes in Electroencephalogram in Alzheimer's Disease. Complexity 2018.
Babiloni, C., Frisoni, G.B., Pievani, M., et al., 2009. Hippocampal volume and cortical sources of EEG alpha rhythms in mild cognitive impairment and Alzheimer disease. Neuroimage 44, 123–135.
Babiloni, C., Lizio, R., Del Percio, C., et al., 2013. Cortical sources of resting state EEG rhythms are sensitive to the progression of early stage Alzheimer's disease. J Alzheimers Dis 34, 1015–1035.
Babiloni, C., Carducci, F., Lizio, R., et al., 2013. Resting state cortical electroencephalographic rhythms are related to gray matter volume in subjects with mild cognitive impairment and Alzheimer's disease. Hum Brain Mapp 34, 1427–1446.
Babiloni, C., Del Percio, C., Caroli, A., et al., 2016. Cortical sources of resting state EEG rhythms are related to brain hypometabolism in subjects with Alzheimer's disease: an EEG-PET study. Neurobiol Aging 48, 122–134.
Babiloni, C., Barry, R.J., Basar, E., et al., 2020. International Federation of Clinical Neurophysiology (IFCN) - EEG research workgroup: Recommendations on frequency and topographic analysis of resting state EEG rhythms. Part 1: Applications in clinical research studies. Clin Neurophysiol 131, 285–307.
Beckmann, C.F., DeLuca, M., Devlin, J.T., Smith, S.M., 2005. Investigations into resting-state connectivity using independent component analysis. Philos T R Soc B 360, 1001–1013.
Cai, L., Deng, B., Wei, X., Wang, R., Wang, J., 2018. Analysis of Spontaneous EEG Activity in Alzheimer's Disease Using Weighted Visibility Graph. Conf Proc IEEE Eng Med Biol Soc 2018, 3100–3103.
Canu, E., Agosta, F., Mandic-Stojmenovic, G., et al., 2017. Multiparametric MRI to distinguish early onset Alzheimer's disease and behavioural variant of frontotemporal dementia. Neuroimage Clin 15, 428–438.
Caso, F., Cursi, M., Magnani, G., et al., 2012. Quantitative EEG and LORETA: valuable tools in discerning FTD from AD? Neurobiol Aging 33, 2343–2356.
Cassani, R., Estarellas, M., San-Martin, R., Fraga, F.J., Falk, T.H., 2018. Systematic Review on Resting-State EEG for Alzheimer's Disease Diagnosis and Progression Assessment. Dis Markers 2018, 5174815.
Choi, J., Ku, B., You, Y.G., et al., 2019. Resting-state prefrontal EEG biomarkers in correlation with MMSE scores in elderly individuals. Sci Rep-Uk 9.
D'Amelio, M., Rossini, P.M., 2012. Brain excitability and connectivity of neuronal assemblies in Alzheimer's disease: from animal models to human findings. Prog Neurobiol 99, 42–60.
de Wilde, M.C., Overk, C.R., Sijben, J.W., Masliah, E., 2016. Meta-analysis of synaptic pathology in Alzheimer's disease reveals selective molecular vesicular machinery vulnerability. Alzheimers Dement 12, 633–644.
delEtoile, J., Adeli, H., 2017. Graph Theory and Brain Connectivity in Alzheimer's Disease. Neuroscientist 23, 616–626.
Filippi, M., Basaia, S., Canu, E., et al., 2020. Changes in functional and structural brain connectome along the Alzheimer's disease continuum. Mol Psychiatry 25, 230–239.
Folstein, M.F., Folstein, S.E., McHugh, P.R., 1975. "Mini-mental state". A practical method for grading the cognitive state of patients for the clinician. J Psychiatr Res 12, 189–198.
Gianotti, L.R., Kunig, G., Lehmann, D., et al., 2007. Correlation between disease severity and brain electric LORETA tomography in Alzheimer's disease. Clin Neurophysiol 118, 186–196.
Hanley, J.A., McNeil, B.J., 1983. A method of comparing the areas under receiver operating characteristic curves derived from the same cases. Radiology 148, 839–843.
Hata, M., Tanaka, T., Kazui, H., et al., 2017. Cerebrospinal Fluid Biomarkers of Alzheimer's Disease Correlate With Electroencephalography Parameters Assessed by Exact Low-Resolution Electromagnetic Tomography (eLORETA). Clin EEG Neurosci 48, 338–347.
Jack Jr., C.R., Bennett, D.A., Blennow, K., et al., 2018. NIA-AA Research Framework: Toward a biological definition of Alzheimer's disease. Alzheimers Dement 14, 535–562.
Jones, D.T., Knopman, D.S., Gunter, J.L., et al., 2016. Cascading network failure across the Alzheimer's disease spectrum. Brain 139, 547–562.
Jorge, J., van der Zwaag, W., Figueiredo, P., 2014. EEG-fMRI integration for the study of human brain function. Neuroimage 102 (Pt 1), 24–34.
Jovicich, J., Babiloni, C., Ferrari, C., et al., 2019. Two-Year Longitudinal Monitoring of Amnestic Mild Cognitive Impairment Patients with Prodromal Alzheimer's Disease Using Topographical Biomarkers Derived from Functional Magnetic Resonance Imaging and Electroencephalographic Activity. J Alzheimers Dis 69, 15–35.
Knopman, D.S., DeKosky, S.T., Cummings, J.L., et al., 2001. Practice parameter: diagnosis of dementia (an evidence-based review). Report of the Quality Standards Subcommittee of the American Academy of Neurology. Neurology 56, 1143–1153.
Laufs, H., Krakow, K., Sterzer, P., et al., 2003. Electroencephalographic signatures of attentional and cognitive default modes in spontaneous brain activity fluctuations at rest. Proc Natl Acad Sci U S A 100, 11053–11058.
Lazarou, I., Georgiadis, K., Nikolopoulos, S., et al., 2020. A Novel Connectome-Based Electrophysiological Study of Subjective Cognitive Decline Related to Alzheimer's Disease by Using Resting-State High-Density EEG EGI GES 300. Brain Sci 10, 392.
Mazzeo, S., Santangelo, R., Bernasconi, M.P., et al., 2016. Combining Cerebrospinal Fluid Biomarkers and Neuropsychological Assessment: A Simple and Cost-Effective Algorithm to Predict the Progression from Mild Cognitive Impairment to Alzheimer's Disease Dementia. J Alzheimers Dis 54, 1495–1508.
McKhann, G.M., Knopman, D.S., Chertkow, H., et al., 2011. The diagnosis of dementia due to Alzheimer's disease: recommendations from the National Institute on Aging-Alzheimer's Association workgroups on diagnostic guidelines for Alzheimer's disease. Alzheimers Dement 7, 263–269.
Pascual-Marqui RD, 2007b. Instantaneous and lagged measurements of linear and nonlinear dependence between groups of multivariate time series: frequency decomposition. arXiv:0711.1455 [stat.ME], 2007-November-09. Available at: http://arxiv.org/abs/0711.1455.
Pascual-Marqui RD, 2007a. Discrete, 3D distributed, linear imaging methods of electric neuronal activity. Part 1: exact, zero error localization. arXiv:0710.3341 [math-ph], 2007-October-17. Available at: http://arxiv.org/pdf/0710.3341.
Pascual-Marqui, R.D., Lehmann, D., Koukkou, M., et al., 2011. Assessing interactions in the brain with exact low-resolution electromagnetic tomography. Philos T R Soc A 369, 3768–3784.
Qiu, C., Kivipelto, M., von Strauss, E., 2009. Epidemiology of Alzheimer's disease: occurrence, determinants, and strategies toward intervention. Dialogues Clin Neurosci 11, 111–128.
Rossini, P.M., Di Iorio, R., Vecchio, F., et al., 2020. Early diagnosis of Alzheimer's disease: the role of biomarkers including advanced EEG signal analysis. Report from the IFCN-sponsored panel of experts. Clin Neurophysiol 131, 1287–1310.
Rubinov, M., Sporns, O., 2010. Complex network measures of brain connectivity: uses and interpretations. Neuroimage 52, 1059–1069.
Santangelo, R., Dell'Edera, A., Sala, A., et al., 2019. The CSF p-tau181/Abeta42 Ratio Offers a Good Accuracy "In Vivo" in the Differential Diagnosis of Alzheimer's Dementia. Curr Alzheimer Res 16, 587–595.
Schurmann, M., Basar, E., 2001. Functional aspects of alpha oscillations in the EEG. Int J Psychophysiol 39, 151–158.
Shirer, W.R., Ryali, S., Rykhlevskaia, E., Menon, V., Greicius, M.D., 2012. Decoding subject-driven cognitive states with whole-brain connectivity patterns. Cereb Cortex 22, 158–165.
Smailovic, U., Jelic, V., 2019. Neurophysiological Markers of Alzheimer's Disease: Quantitative EEG Approach. Neurol Ther 8, 37–55.
Smailovic, U., Koenig, T., Kareholt, I., et al., 2018. Quantitative EEG power and synchronization correlate with Alzheimer's disease CSF biomarkers. Neurobiol Aging 63, 88–95.
Smith, S.M., Nichols, T.E., 2009. Threshold-free cluster enhancement: addressing problems of smoothing, threshold dependence and localisation in cluster inference. Neuroimage 44, 83–98.
Sporns, O., Chialvo, D.R., Kaiser, M., Hilgetag, C.C., 2004. Organization, development and function of complex brain networks. Trends Cogn Sci 8, 418–425.
Stam, C.J., Pijn, J.P., Suffczynski, P., Lopes da Silva, F.H., 1999. Dynamics of the human alpha rhythm: evidence for non-linearity? Clin Neurophysiol 110, 1801–1813.
Tijms, B.M., Wink, A.M., de Haan, W., et al., 2013. Alzheimer's disease: connecting findings from graph theoretical studies of brain networks. Neurobiol Aging 34, 2023–2036.
Vecchio, F., Miraglia, F., Marra, C., et al., 2014. Human brain networks in cognitive decline: a graph theoretical analysis of cortical connectivity from EEG data. J Alzheimers Dis 41, 113–127.
Vecchio, F., Miraglia, F., Curcio, G., et al., 2015. Cortical brain connectivity evaluated by graph theory in dementia: a correlation study between functional and structural data. J Alzheimers Dis 45, 745–756.
Vecchio, F., Miraglia, F., Maria, Rossini P., 2017. Connectome: Graph theory application in functional brain network architecture. Clin Neurophysiol Pract 2, 206–213.
Vecchio, F., Miraglia, F., Iberite, F., et al., 2018. Sustainable method for Alzheimer dementia prediction in mild cognitive impairment: Electroencephalographic connectivity and graph theory combined with apolipoprotein E. Ann Neurol 84, 302–314.
Xie, T., He, Y., 2011. Mapping the Alzheimer's brain with connectomics. Front Psychiatry 2, 77.
Zhang, H.Y., Wang, S.J., Liu, B., et al., 2010. Resting brain connectivity: changes during the progress of Alzheimer disease. Radiology 256, 598–606.
Zhou, J., Liu, S., Ng, K.K., Wang, J., 2017. Applications of Resting-State Functional Connectivity to Neurodegenerative Disease. Neuroimaging Clin N Am 27, 663–683.